Two-dimensional Niobate Nanosheet Membranes for Water Treatment: Effect of Nanosheet Preparation Method on Membrane Performance

Nakagawa, Keizo ; Sera, Tomohiro ; Kunimatsu, Misato ; Yamashita, Hiroharu ; Yoshioka, Tomohisa ; Shintani, Takuji ; Kamio, Eiji ; Tsang…

(Citation)
Separation and Purification Technology,219:222-229

(Issue Date)
2019-07-15

(Resource Type)
journal article

(Version)
Accepted Manuscript

(URL)
https://hdl.handle.net/20.500.14094/90008087

Two-dimensional Niobate Nanosheet Membranes for Water Treatment: Effect of Nanosheet Preparation Method on Membrane Performance

Keizo Nakagawa[1]*, Tomohiro Sera[1], Misato Kunimatsu[2], Hiroharu Yamashita[2], Tomohisa Yoshioka[1], Takuji Shintani[1], Eiji Kamio[2], Shik Chi Edman Tsang[3] and Hideto Matsuyama[1,2]*

[1]*Center for Membrane and Film Technology, Graduate School of Science, Technology and Innovation, Kobe University, 1-1 Rokkodai, Nada, Kobe 657-8501, Japan.*

[2]*Center for Membrane and Film Technology, Department of Chemical Science and Engineering, Kobe University, 1-1 Rokkodai, Nada, Kobe 657-8501, Japan.*

[3]*Wolfson Catalysis Centre, Department of Chemistry, University of Oxford, South Parks Road, Oxford, OX1 3QR, UK.*

*Corresponding author. Tel & Fax: +81-78-803-6302

E-mail address: knakagaw@port.kobe-u.ac.jp (K. Nakagawa)

matuyama@kobe-u.ac.jp (H. Matsuyama)

Abstract

Niobate nanosheet membranes were fabricated by vacuum filtration using niobate nanosheets prepared by the hydrothermal method (HT-NbO membranes) and the exfoliation method (EX-NbO membranes). Membrane structure, water permeance and separation performance for these membrane types were measured and compared. Both membrane types had a dense structure and retained high structural stability in water *via* chemical cross-linking between sheets. The difference of the intercalated molecules and interaction between nanosheets affected the interlayer distance of the membranes. As a result, higher water permeance but lower rejection of polyethylene glycol, Na_2SO_4 and Acid Red 265 was observed for EX-NbO membranes than for HT-NbO membranes. This is due to the formation of larger nanochannels in EX-NbO membranes. A model of a water pathway through nanochannels based on void structure proposed for the HT-NbO membranes can also be applied for EX-NbO membranes.

Keywords: niobate nanosheet membrane; hydrothermal method; exfoliation method; nanofiltration; water treatment

1. Introduction

Two-dimensional (2D) nanosheet membranes, such as graphene-based, are expected to function as size-selective molecular separation membranes, based on their unique atomic thickness with micrometer lateral dimensions. Different types of separation membranes using 2D nanosheets have been studied, including nanosheet composite membranes [1–4], porous nanosheet membranes [5–7] and stacked nanosheet membranes [8–19]. Stacked nanosheet membranes have been widely studied because of their separation capability using tunable 2D nanochannels, electrostatic interaction, and adsorption properties of the nanosheets. Stacked nanosheet membranes are formed by assembling nanosheets into ultrathin membranes containing nanochannels between the stacked sheets that allow water to pass through while rejecting unwanted solutes. In addition, stacked nanosheet membranes are relatively easy to fabricate via various processes including vacuum filtration [8,9,12–14], vacuum suction [15], pressure-assisted filtration [16], spin casting [17], the layer-by-layer approach [18,19], the wet phase inversion method [10] or spray coating [11]. In addition, a wide variety of nanosheet materials and support membranes are available. Most studies to-date have fabricated graphene-based membranes with high flux and separation performance. However, only a narrow range of nanosheet materials, such as graphene oxide (GO) [8–19], transition metal dichalcogenides [20–23] and transition metal oxides [24,25] have been studied for membrane preparation, although many other nanosheet materials have been reported. Transition metal oxide nanosheets offer attractive surface and catalytic properties [26–31]; therefore, they represent promising materials for potentially high-functioning

membranes.

Recently, we developed stacked nanosheet membranes using single molecular sheets of niobate. The membranes were prepared with a bottom-up approach using the hydrothermal method [25]. Results showed that the niobate nanosheet membranes demonstrated high structural stability in water via chemical cross-linking between their sheets and superior nanofiltration performance when compared with graphene oxide membranes fabricated by a similar vacuum filtration method [25]. The most common preparation method of 2D metal oxide nanosheets is a top-down approach using the exfoliation method [26–28]. Typically, multi-layered bulk compounds can be exfoliated by first intercalating their layers with base molecules, followed by rupturing these layered structures to yield unilaminar colloids. The lateral size of crystallite nanosheets and the chemical agents in the colloidal metal oxide nanosheet solution depend on the preparation methods. To fabricate various kinds of nanosheet membranes with good separation performance and functionality using metal oxide nanosheets, it is important to study the effects of nanosheet preparation method on membrane performance. In this study, stacked nanosheet membranes were fabricated using niobate nanosheets prepared by the hydrothermal and exfoliation methods. Membrane structure and the performance of the stacked niobate nanosheet membranes were evaluated and compared.

2. Experimental

2.1 Materials

All chemicals used in this study were analytical grade with over 99% purity and were obtained from Wako Pure Chemical Industries, Osaka, Japan unless otherwise stated. All aqueous solutions were prepared with Milli-Q water (> 18.2 MΩ cm, Merck Millipore, Billerica, MA, USA).

2.2 Preparation of single layer niobate nanosheets by the hydrothermal method (bottom-up approach)

Niobate molecular sheets were synthesized by the hydrothermal method using amine surfactants in ammonia solution [29]. In this experiment, 1.989 g of niobium(V) ethoxide ($Nb(OEt)_5$) (Kojundo Chemical Laboratory Co., Ltd., Saitama, Japan) (0.00625 mol) was mixed with 3.735 g of triethanolamine (TEOA) (0.025 mol), which is stable against hydrolysis at room temperature. The mixed solution was added to 25 mL of NH_3 aqueous solution and the final pH of the mixture was at 12.8 which is close to NH_3 aqueous solution itself because the volume of NH_3 aqueous solution was larger than that of the mixed solution of $Nb(OEt)_5$ and TEOA. The mixture was then transferred to a 45 mL Teflon autoclave, and processed at 160 °C for 24 h. During hydrothermal synthesis, chemical reactions between $Nb(OEt)_5$ and water result in the nucleation and growth of niobium oxide. To control the evolution of the 2D niobium oxide structure and morphology, TEOA was used as an adsorbing–chelating ligand for $Nb(OEt)_5$, stabilizing Nb against rapid hydrolysis in an alkaline solution. As a result, the single-molecular layered sheets were stabilized against stacking [29]. The resulting product was centrifuged at 6000 rpm for 10 min, to obtain a colloidal suspension with a small amount of white

precipitate. The precipitate fraction was removed and the supernatant colloid was collected as the final product.

2.3 Preparation of single layer niobate nanosheets by the exfoliation method (top-down approach)

Niobate molecular sheets were prepared by the conventional exfoliation method using tetra(*n*-butylammonium) hydroxide (TBAOH; Sigma-Aldrich Corp., St. Louis, MO, USA) from layered niobate [26–28]. For this experiment, K_2CO_3 and Nb_2O_5 were mixed in molar ratios of 1.1:3 and calcined at 600 °C for 2 h, then at 900 °C for 3 h to synthesize KNb_3O_8. The obtained KNb_3O_8 was converted to $H_3ONb_3O_8$ by immersion in 6.0 M HCl at 60 °C for 1 week. The acid solution was replaced with fresh solutions daily. The resulting precipitate was filtered, washed with distilled water repeatedly until the filtrate became pH-neutral and then dried at 60 °C overnight (~12 h). The obtained $H_3ONb_3O_8$ was converted to HNb_3O_8 by calcination at 150 °C for 3 h. Exfoliated niobate molecular sheets were prepared by first adding 15 wt% TBAOH solution to 100 mL of distilled water containing 20 mg of HNb_3O_8. The resulting suspension was adjusted to a pH of 9.0–10.0 and shaken for 3–5 days. The resulting product was centrifuged at 6000 rpm for 10 min to obtain a colloidal suspension with white precipitate. The precipitate was removed and the supernatant colloid was collected as the final product.

2.4 Fabrication of stacked nanosheet membranes by vacuum filtration

Stacked niobate nanosheet membranes were fabricated by vacuum filtration [25] on a surface-modified porous cellulose nitrate (CN) support (Millipore Corp.) using each nanosheet colloidal solution. A CN support with a pore size of 50 nm was immersed in a solution containing 2.5 vol% 3-aminopropyl-triethoxysilane (APTES; Shin-Etsu Chemical Co., Tokyo, Japan) for 30 min, then removed and immersed into Milli-Q water for 30 minutes. After washing with 100 mL of Milli-Q water using a vacuum filtration system, the modified support (denoted CN-APTES) was used to fabricate the stacked niobate nanosheet membranes. The membranes were assembled by vacuum filtration of a given nanosheet colloidal solution, prepared by the exfoliation method or the hydrothermal method, on the CN-APTES. Typically, 50 mL of 0.337 mg/L nanosheet colloidal solution yielded a membrane with a thickness of approximately 90 nm. The thickness of the NbO membranes was controlled by adjusting the volume of nanosheet colloidal solution used during the vacuum filtration. Prepared membranes were vacuum dried at 25 °C for two hours to remove water and strengthen the adhesion between nanosheets. The stacked nanosheet membranes obtained from nanosheet colloidal solutions prepared by the exfoliation method and the hydrothermal method are denoted as EX-NbO and HT-NbO membranes, respectively.

2.5 Membrane Characterization

The crystalline phases of the samples were identified by powder X-ray diffraction (XRD) (RINT

2500 VHF, Rigaku Corp.) with monochromatized Cu Kα radiation at 40 kV and 40 mA. Transmission electron microscope (TEM) images of the membrane samples were recorded using a JEM-2100F electron microscope (JEOL Ltd.). Field Emission Scanning Electron Microscope (FE-SEM) images of the samples were recorded using a JSF-7500F electron microscope (JEOL Ltd.). Atomic force microscopy (AFM) images were recorded with an SPA-400 (Hitachi High-Tech Science). The AFM observations were carried out with an OMCL-AC160TS-C3 cantilever (OLYMPUS) in dynamic force mode. The ζ-potentials of the sample surfaces were measured with an electrophoretic light-scattering apparatus (ELSZ-1000; Photal Otsuka Electronics) using a flat quartz cell in aqueous NaCl (10 mmol/L) at a pH of 6.7. The chemical composition of the membrane surfaces was analyzed with XPS (JPS-9200, JEOL Ltd.).

2.6 Evaluation of membrane performance

Membrane performance was evaluated with a cross-flow membrane filtration system [25]. This system was composed of a membrane cell, pump (PCS Pump, SP-22-32-P; FLOM, Inc.) to control the feed water flow rate, back pressure valve to control the applied pressure, feed reservoir, permeate reservoir and condensate reservoir. The effective area of the sample membranes was 7.07×10^{-4} m^2. The feed water flow rate and applied pressure were 1.0 mL/min and 0.4 MPa, respectively. To evaluate pressure-dependent water flux, the applied pressure was adjusted from 0.1 to 1.0 MPa. The applied pressure time was kept at 30 min for the tests of pressure-dependent water flux. The feed water side of

the membrane cell was continuously stirred by a magnetic stirrer. The water permeance of the membranes was evaluated using Milli-Q water as the feed solution, and calculated from the mass increase of permeate. For each experimental condition, data was collected from a minimum of three independently-fabricated samples and averaged.

Membrane performance was also evaluated based on the rejection of polyethylene glycol (PEG; Sigma-Aldrich Corp., St. Louis, MO, USA). Aqueous solutions containing 1.0 g/L of one of five molecular weights (Mw) of PEG (1, 2, 6, 12, 14 and 20 kDa) and 0.01 g/L of NaCl as a reference material were used as the feed solutions. The concentration of NaCl in the permeate was analyzed using a conductivity meter (LAQUAtwin B-722; HORIBA, Ltd). Once the permeate NaCl concentration was stable, the PEG concentration in the permeate was analyzed using a total organic carbon analyzer (TOC-V_{CSH}; Shimadzu Co.). The rejection of Evans blue (EB, Mw: 960.8) and Acid red 265 (AR265; Tokyo Chemical Industries, Tokyo, Japan, Mw: 635.6) were also examined. Aqueous solutions containing 10 ppm of EB and AR265 were used as the feed solutions. The concentrations of EB and AR265 in solution were estimated by measuring the absorbance, which was maximized at approximately λ = 609 nm for EB and 542 nm for AR265, with a UV/Vis spectrophotometer (V-650, JASCO International Co., Ltd). To measure salt rejection, an aqueous solution of 500 ppm each NaCl and Na_2SO_4 was used as the feed water. The concentration of each NaCl and Na_2SO_4 in the permeate was analyzed using a conductivity meter (LAQUAtwin B-722; HORIBA, Ltd.). The rejection (R) of each solute was calculated from the following equation: R (%) = (1 - C_P / C_F) × 100, where C_F and C_P

are the concentrations of the feed and the permeate solutions, respectively.

3. Results and discussion

3.1. Fabrication of niobate nanosheet membranes using colloidal nanosheets prepared by different methods

Single-molecular layers of niobate nanosheets were prepared by the conventional exfoliation method using TBAOH from layered niobate, and the hydrothermal method in the presence of TEOA. According to XRD patterns (Fig. S1), HNb_3O_8 is a highly crystalline material consisting of alternating layers of negatively charged NbO_6 octahedra and protons [27,28]. The niobate nanosheet materials synthesized by hydrothermal method show similar diffraction patterns to those of HNb_3O_8; however, the peaks are much broader (Fig. S1). This indicates that they share the basic structural features of HNb_3O_8, but their layer thickness and structural order have been greatly reduced [29]. Subsequently, the niobate nanosheets were assembled by vacuum filtration on the modified CN support. Structural analyses of the prepared samples and membranes were carried out by TEM, FE-SEM and XRD.

Fig. 1 shows TEM images and sheet size distributions (including the averages) of the niobate nanosheets prepared by the exfoliation method and the hydrothermal method. Distinct flat, single-molecular sheet layers with sharp edges were observed for both preparation methods. The average size of nanosheets prepared by the hydrothermal method was 40 nm. In contrast, the average size of nanosheets prepared by the exfoliation method was 115 nm, three times larger than those prepared by

the hydrothermal method. A few larger (200–300 nm) nanosheets were also created by the exfoliation method. The standard deviation (σ) of the nanosheet size by the hydrothermal method (15.4 nm) was smaller than that of nanosheets prepared by the exfoliation method (74.2 nm). These results indicate that more uniformly-sized nanosheets are obtained when prepared by the hydrothermal method. The thickness of both niobate nanosheets has been characterized by AFM (Fig. S2). Considering that thickness of HNb_3O_8 monolayer is 0.9 nm and the thickness evaluation includes experimental errors, the sheets are estimated to be single or a few layers.

Fig. 2 shows the overview and cross-sectional SEM images of examples of the fabricated HT-NbO and EX-NbO membranes. The overview SEM images show smooth surfaces on both membrane types and a relatively flat surface for the EX-NbO membrane. The cross-section images show that the nanosheets were stacked on the support, and the total thickness of the membranes was approximately 30 nm for the HT-NbO and 100 nm for the EX-NbO membranes. Both types of NbO nanosheets appear to be interconnected and form a flat, thin layer on the modified support.

Fig. 3 shows the XRD patterns of both NbO membrane types at a membrane thickness of approximately 100 nm in dry and wet conditions. In dry conditions, diffraction peaks of the (010) plane derived from the interlayer spacing of the stacked membranes were observed at around $2\theta = 6 - 10$ °. For the EX-NbO membrane, a larger interlayer spacing (1.2 nm) was obtained than for the HT-NbO membrane (1.0 nm). It is assumed that the difference in the interlayer spacing is due to the species of intercalated molecules, namely TEOA molecules for the HT-NbO membrane and TBA cations for the

EX-NbO membrane. A sharper peak was obtained for the EX-NbO membrane. It is possible that a higher ordered stacked structure was produced for the EX-NbO membrane because larger-sized nanosheets would more easily stack regularly on the support layer than smaller-sized nanosheets; this is consistent with the flat surface observed in the SEM image (Fig. 2b). On the other hand, when inspecting the structural differences in the XRD patterns between dry and wet conditions, only slight increases in the interlayer distance were observed for both membranes following immersion. These results clearly indicate that both membranes retain high structural stability in water, and the GO membranes are easily peeled off of the support [25,32]. Considering that the thickness of a single niobate sheet is 0.9 nm [29] and the interlayer distances in wet conditions, as estimated with XRD, were 1.1 nm for the HT-NbO membrane and 1.3 nm for the EX-NbO membrane, the free spacing between sheet layers was calculated as 0.2 nm for the HT-NbO membrane and 0.4 nm for the EX-NbO membrane, respectively.

Therefore, vacuum filtration using niobate nanosheet colloidal solution created both types of NbO membranes with dense and highly stable structures in water. We previously reported that the surface acidity of the niobate nanosheets and the amine-containing chemical binders enhanced the structural stability in the membranes [25]. With respect to the interaction between the nanosheets and the CN-APTES support, the ethoxy groups of the APTES reacted with the surface hydroxyl groups of the cellulose in the CN support during the pretreatment of the support with APTES. In our previous study [24], niobate nanosheets behaved as strong solid acids, possessing both Brønsted and Lewis acid sites,

and thereby acted as solid acid catalysts [30,31]. Therefore, the amino groups of the APTES reacted with the niobate nanosheets via both coordination bonding and hydrogen bonding during the vacuum filtration and drying processes, resulting in an enhanced interaction between the niobate nanosheets and the CN-APTES support [25]. It was assumed that the interactions between the nanosheet layers would be different for HT-NbO and EX-NbO membranes. TEOA molecules effectively crosslink the sheet layers via coordination bonding and hydrogen bonding for HT-NbO membranes [25]. In contrast, TBA cations, used for the exfoliation of nanosheets from the bulkier HNb_3O_8, would exist in the interlayers of nanosheets via electrostatic interaction for EX-NbO membranes. XPS analysis provides evidence for the existence of TBA ions in the prepared membranes, as shown in Fig. S3. Thus, the type of intercalated molecules and the interactions between sheet layers strongly affect the interlayer distance within the membranes.

3.2. Performance of niobate nanosheet membranes

Fig. 4 shows the water permeance and rejection of PEG with different molecular weight for each NbO membrane. The tests were carried out using the cross-flow membrane system described in section 2.6. For the controlled test of membrane performance, the bare CN support without NbO nanosheets showed water permeance of around 400 $LMH \cdot bar^{-1}$ and extremely low rejection for PEG with molecular weights from 1 to 20 kDa [25]. Results show that higher water permeance was obtained for EX-NbO membranes (5.7 $LMH \cdot bar^{-1}$) when compared to HT-NbO membranes (3.0 $LMH \cdot bar^{-1}$), at a

membrane thickness of 40–50 nm (Fig. 4a). The molecular weight cutoffs (MWCOs) of the membranes were measured using PEG of a range of molecular weights (Fig. 4b). The results indicated that the MWCO (i.e., the Mw at which 90% rejection was achieved) was 4.3 kDa for HT-NbO membranes. The MWCO could not be estimated by PEG for the EX-NbO membranes because of the lower rejection of PEG. The Stokes–Einstein radii [33] is estimated as 1.7 nm for 4.3 kDa of PEG. Thus, from the MWCO measurements using PEG, it was concluded that nanochannels with diameters of 3.4 nm were formed in the HT-NbO membranes and nanochannels with diameters larger than 3.4 nm were formed in the EX-NbO membranes.

The rejection performance of the membranes was further studied using anionic dyes (EB and AR 265), and salts (Na_2SO_4 and NaCl), as shown in Fig. 5. Both NbO membranes demonstrated rejection of greater than 90% for AR 265 and EB. Although the rejection of NaCl was approximately 5% for both NbO membranes, the HT-NbO membranes showed higher rejection of Na_2SO_4 and AR 265 than the EX-NbO membranes. The surface charge (ζ-potentials) of the NbO membranes at several pH levels were measured by streaming potential measurements (Fig. 6a). The effects of surface charge on NaCl and Na_2SO_4 rejection at various pH levels was also investigated (Fig. 6b). The ζ-potentials were found to be dependent on pH, with an iso-electric point (IEP) of approximately 4.0 for HT-NbO membranes; this was slightly lower than that for EX-NbO membranes (4.5). In addition, the values of ζ-potentials for EX-NbO membranes were higher than those for HT-NbO membranes at all tested pH values. This is because the cationic TBA molecules were intercalated into the interlayers via electrostatic interaction,

and the negative surface charge of niobate nanosheets was slightly weakened in the EX-NbO membranes. Both types of NbO membranes became negatively charged above the IEP values. As the membrane surface charge became increasingly negative, the rejection of NaCl and Na_2SO_4 increased. The negatively charged NbO membranes displayed a greater rejection of multivalent than monovalent anions, consistent with the Donnan exclusion mechanism [34,35].

In the HT-NbO membranes, the free spacing between the NbO sheets was estimated at only 0.2 nm based on the XRD results. This spacing did not substantially increase in the presence of water because the TEOA acted as a chemical binder between sheets, preventing water from entering the interlayers. We had previously suggested the formation of nanochannels originating from a void structure as the water pathway through the membrane [25] (Fig.7). This void structure is created when the sheets are stacked and water passes through the thin membranes during vacuum filtration. For EX-NbO membranes, the free spacing between sheet layers was estimated at 0.4 nm; this spacing might be large enough for water molecules to pass through the interlayer. However, exceptionally high water permeance could not be obtained for EX-NbO membrane although the EX-NbO membrane showed higher water permeance than the HT-NbO membrane. In addition, the sterically bulky TBA molecules are intercalated into the interlayers. Thus, the water pathway model proposed for the HT-NbO membrane, based on nanochannels from a void structure is also applicable for EX-NbO membranes. A simplified schematic diagram showing the different void structures formed between stacked nanosheets for HT-NbO and EX-NbO membranes is depicted in Fig.7. Although the two membrane

types have only 0.2 nm difference of free spacing between them, the channel size for EX-NbO membranes is considered to be larger than that for HT-NbO membranes (> 3.4 nm) as the created channel size corresponds to the number of layers and interlayers. In the case of GO membranes, it has been reported that reducing the sheet size can shorten the molecular transport pathway and increase of the water permeability, but it does not affect their water/salt selectivity because the interlayer spacing does not change [13]. For NbO membranes, reducing the sheet size may shorten the water transport pathway and increase the pore volume, and these factors have possibilities to contribute to increase the water permeance, while the reducing the sheet size does not affect the separation performance considering from the water pathway model of nanochannels from a void structure. However, HT-NbO membranes showed lower water permeance than EX-NbO membranes (Fig. 4a). Therefore, the difference of the stacked structure (size of free spacing and periodicity) rather than the sheet size would affect the water permeance.

3.3. Pressure-dependent water flux of niobate nanosheet membranes

Pressure-dependent water flux was investigated to confirm the rigidity of the nanochannels of the NbO membranes due to of the importance of membrane durability. NbO membranes with a membrane thickness of 40–50 nm were studied. The water flux of HT-NbO membranes under pressures from 1 bar to 10 bar is shown in Fig. 8a. Water flux increases proportionally with applied pressure until 9 bar, suggesting that the nanochannels are rigid enough to withstand external pressure up to 9 bar. Based on

the typical viscous flow according to the Hagen–Poiseuille equation [9], water flux is proportional to the differential pressure. The water flows through the void structure between niobate nanosheets as shown in Fig.7. This indicates that the channels in the HT-NbO membrane do not swell and shrink, even under an applied pressure up to 9 bar. An unexpected increase in water flux at 10 bar applied pressure was observed. Below this pressure, the water flux decreases linearly with decreasing external pressure (line 2 in Fig. 8a). When the pressure returns back to 1 bar, the water flux is nearly the same as in the original membrane state. When the external pressure increases again (line 3 in Fig. 8a), water permeance increases proportionally with the applied pressure until 10 bar. The transition at 10 bar of line 1 in Fig. 8a implies that only a slight geometrical change of the nanochannels occurred during the pressure loading on the membranes beyond 9 bar.

Alternatively, the EX-NbO membranes display a different trend between pressure and water flux. The water flux of EX-NbO membranes from pressures of 1 bar to 6 bar is shown in Fig. 8b. At low pressures, the water flux increases linearly with external pressure, then remains constant at pressures of 3–4 bar, and slightly decreases until 6 bar (line 1 in Fig. 8b). After 6 bar, the applied pressure was reduced in order to prevent the membrane from unexpected collapsing. This limited water flux behavior against pressure loading has been reported for GO membranes [8]. The nanochannels of GO membranes collapse and shrink at high pressure, but recover if the applied pressure is released, due to their mechanically elastic property. In the case of EX-NbO membranes, the nanochannels seem to be shrunk at high pressure loading. The transformed nanochannels do not recover upon release of the

applied pressure (lines 2–4 in Fig. 8b) because of the rigidity of the niobate nanosheets, which differs from GO membranes. However, it should be noted that in the pressure loading cycle experiment, the water flux increased linearly with the applied pressure. These results imply that the nanochannels in EX-NbO membranes would function stably after 6 bar applied pressure was added to the membrane. For the test of pressure-dependent water flux, the experimental conditions such as applied pressure as well as applied pressure time affect their membrane permeation. Water flux sometimes shows sensitive response to the applied pressure time at each applied pressure in the case that membrane structure is less stable. Further study is necessary to clarify the stability of the stacked structure against such high applied pressure.

4. Conclusions

Stacked niobate nanosheet membranes were fabricated using niobate nanosheets prepared by hydrothermal or exfoliation methods. It was found that both membrane types had a dense structure and retained high structural stability in water. Both niobate nanosheet membranes act as nanofiltration membranes with excellent rejection performances against anionic dyes and salts. Higher water permeance but lower rejection of neutral molecule (PEG) and anionic species (Na_2SO_4 and Acid Red 265) was observed for EX-NbO membranes than for HT-NbO membranes because of the formation of larger nanochannels in EX-NbO membranes. Differences in membrane performance are attributed to the type of intercalated molecules and interaction between layers for each niobate nanosheet membrane.

The pressure loading cycle experiment show the potential durability of NbO membranes. Because various kinds of metal oxide nanosheets can be prepared by exfoliation method, these results are expandable to the fabrication of novel metal oxide nanosheet membranes with superior functionality.

Acknowledgments

This work was supported by JSPS KAKENHI Grant Number JP16K06829 and Kurita Water and Environment Foundation Grant Number 16A078.

References

[1] P. Gorgojo, D. Sieffert, C. Staudt, C. Tellez, J. Coronas, Exfoliated zeolite Nu-6(2) as filler for 6FDA-based copolyimide mixed matrix membranes, J. Memb. Sci. 411–412 (2012) 146–152. doi:10.1016/j.memsci.2012.04.025.

[2] T. Rodenas, I. Luz, G. Prieto, B. Seoane, H. Miro, A. Corma, F. Kapteijn, F.X. Llabres i Xamena, J. Gascon, Metal-organic framework nanosheets in polymer composite materials for gas separation, Nat. Mater. 14 (2014) 48–55. doi:10.1038/nmat4113.

[3] Y.C. Wang, S.R. Kumar, C.M. Shih, W.S. Hung, Q.F. An, H.C. Hsu, S.H. Huang, S.J. Lue, High permeance nanofiltration thin film composites with a polyelectrolyte complex top layer containing graphene oxide nanosheets, J. Memb. Sci. 540 (2017) 391–400. doi:10.1016/j.memsci.2017.06.074.

[4] Z.X. Low, J. Ji, D. Blumenstock, Y.M. Chew, D. Wolverson, D. Mattia, Fouling resistant 2D boron nitride nanosheet – PES nanofiltration membranes, J. Memb. Sci. 563 (2018) 949–956. doi:10.1016/j.memsci.2018.07.003.

[5] J. Choi, M. Tsapatsis, MCM-22/Silica Selective Flake Nanocomposite Membranes for Hydrogen Separations, J. Am. Chem. Soc. 132 (2010) 448–449. doi:10.1021/ja908864g.

[6] K. Varoon, X. Zhang, B. Elyassi, D.D. Brewer, M. Gettel, S. Kumar, J.A. Lee, S. Maheshwari, A. Mittal, C.-Y. Sung, M. Cococcioni, L.F. Francis, A. V. McCormick, K.A. Mkhoyan, M. Tsapatsis, Dispersible Exfoliated Zeolite Nanosheets and Their Application as a Selective Membrane, Science (80-.). 334 (2011) 72–75. doi:10.1126/science.1208891.

[7] S.P. Surwade, S.N. Smirnov, I. V. Vlassiouk, R.R. Unocic, G.M. Veith, S. Dai, S.M. Mahurin, Water desalination using nanoporous single-layer graphene, Nat. Nanotechnol. 10 (2015) 459–464. doi:10.1038/nnano.2015.37.

[8] H. Huang, Y. Mao, Y. Ying, Y. Liu, L. Sun, X. Peng, Salt concentration, pH and pressure controlled separation of small molecules through lamellar graphene oxide membranes, Chem. Commun. 49 (2013) 5963–5965. doi:10.1039/c3cc41953c.

[9] H. Huang, Z. Song, N. Wei, L. Shi, Y. Mao, Y. Ying, L. Sun, Z. Xu, X. Peng, Ultrafast viscous water flow through nanostrand-channelled graphene oxide membranes, Nat. Commun. 4 (2013) 2979–2987. doi:10.1038/ncomms3979.

[10] R.L.G. Lecaros, G.E.J. Mendoza, W.S. Hung, Q.F. An, A.R. Caparanga, H.A. Tsai, C.C. Hu, K.R. Lee, J.Y. Lai, Tunable interlayer spacing of composite graphene oxide-framework membrane for acetic acid dehydration, Carbon N. Y. 123 (2017) 660–667. doi:10.1016/j.carbon.2017.08.019.

[11] A. Morelos-Gomez, R. Cruz-Silva, H. Muramatsu, J. Ortiz-Medina, T. Araki, T. Fukuyo, S.

Tejima, K. Takeuchi, T. Hayashi, M. Terrones, M. Endo, Effective NaCl and dye rejection of hybrid graphene oxide/graphene layered membranes, Nat. Nanotechnol. 12 (2017) 1083–1088. doi:10.1038/nnano.2017.160.

[12] J. Abraham, K.S. Vasu, C.D. Williams, K. Gopinadhan, Y. Su, C.T. Cherian, J. Dix, E. Prestat, S.J. Haigh, I. V. Grigorieva, P. Carbone, A.K. Geim, R.R. Nair, Tunable sieving of ions using graphene oxide membranes, Nat. Nanotechnol. 12 (2017) 546–550. doi:10.1038/nnano.2017.21.

[13] Y.H. Cho, H.W. Kim, H.D. Lee, J.E. Shin, B.M. Yoo, H.B. Park, Water and ion sorption, diffusion, and transport in graphene oxide membranes revisited, J. Memb. Sci. 544 (2017) 425–435. doi:10.1016/j.memsci.2017.09.043.

[14] J.Y. Chong, B. Wang, K. Li, Water transport through graphene oxide membranes: The roles of driving forces, Chem. Commun. 54 (2018) 2554–2557. doi:10.1039/c7cc09120f.

[15] K. Huang, G. Liu, Y. Lou, Z. Dong, J. Shen, W. Jin, A graphene oxide membrane with highly selective molecular separation of aqueous organic solution, Angew. Chemie - Int. Ed. 53 (2014) 6929–6932. doi:10.1002/anie.201401061.

[16] W.S. Hung, Q.F. An, M. De Guzman, H.Y. Lin, S.H. Huang, W.R. Liu, C.C. Hu, K.R. Lee, J.Y. Lai, Pressure-assisted self-assembly technique for fabricating composite membranes consisting of highly ordered selective laminate layers of amphiphilic graphene oxide, Carbon N. Y. 68 (2014) 670–677. doi:10.1016/j.carbon.2013.11.048.

[17] H.W. Kim, H.W. Yoon, S. Yoon, B.M. Yoo, B.K. Ahn, Y.H. Cho, H.J. Shin, H. Yang, U. Paik, S. Kwon, J.-Y. Choi, H.B. Park, Selective Gas Transport Through Few-Layered Graphene and Graphene Oxide Membranes, Science (80-.). 342 (2013) 91–95. doi:10.1126/science.1236098.

[18] M. Hu, B. Mi, Enabling Graphene Oxide Nanosheets as Water Separation Membranes, Environ. Sci. Technol. 47 (2013) 3715–3723. doi:10.1021/es400571g.

[19] J. Zhao, Y. Zhu, F. Pan, G. He, C. Fang, K. Cao, R. Xing, Z. Jiang, Fabricating graphene oxide-based ultrathin hybrid membrane for pervaporation dehydration via layer-by-layer self-assembly driven by multiple interactions, J. Memb. Sci. 487 (2015) 162–172. doi:10.1016/j.memsci.2015.03.073.

[20] L. Sun, H. Huang, X. Peng, Laminar MoS2 membranes for molecule separation, Chem. Commun. 49 (2013) 10718–10720. doi:10.1039/c3cc46136j.

[21] L. Sun, Y. Ying, H. Huang, Z. Song, Y. Mao, Z. Xu, X. Peng, Ultrafast molecule separation through layered WS2 nanosheet membranes, ACS Nano. 8 (2014) 6304–6311. doi:10.1021/nn501786m.

[22] M. Deng, K. Kwac, M. Li, Y. Jung, H.G. Park, Stability, Molecular Sieving, and Ion Diffusion

Selectivity of a Lamellar Membrane from Two-Dimensional Molybdenum Disulfide, Nano Lett. 17 (2017) 2342–2348. doi:10.1021/acs.nanolett.6b05238.

[23] Z. Wang, Q. Tu, S. Zheng, J.J. Urban, S. Li, B. Mi, Understanding the Aqueous Stability and Filtration Capability of MoS2Membranes, Nano Lett. 17 (2017) 7289–7298. doi:10.1021/acs.nanolett.7b02804.

[24] P. Sun, Q. Chen, X. Li, H. Liu, K. Wang, M. Zhong, J. Wei, D. Wu, R. Ma, T. Sasaki, H. Zhu, Highly efficient quasi-static water desalination using monolayer graphene oxide/titania hybrid laminates, NPG Asia Mater. 7 (2015) e162. doi:10.1038/am.2015.7.

[25] K. Nakagawa, H. Yamashita, D. Saeki, T. Yoshioka, T. Shintani, E. Kamio, H.T. Kreissl, S.C.E. Tsang, S. Sugiyama, H. Matsuyama, Niobate nanosheet membranes with enhanced stability for nanofiltration, Chem. Commun. 53 (2017) 7929–7932. doi:10.1039/C7CC03911E.

[26] A. Takagaki, M. Sugisawa, D. Lu, J.N. Kondo, M. Hara, K. Domen, S. Hayashi, Exfoliated nanosheets as a new strong solid acid catalyst, J. Am. Chem. Soc. 125 (2003) 5479–5485. http://pubs.acs.org/doi/abs/10.1021/ja034085q (accessed January 27, 2014).

[27] A. Takagaki, D. Lu, K. N, Hara Michikazu, S. Hayashi, K. Domen, Exfoliated HNb3O8 nanosheets as a strong protonic solid acid, Chem. Mater. 17 (2005) 2487–2489. http://pubs.acs.org/doi/abs/10.1021/cm047990y (accessed January 22, 2014).

[28] A. Dias, S. Lima, D. Carriazo, V. Rives, M. Pillinger, A.A. Valente, Exfoliated titanate, niobate and titanoniobate nanosheets as solid acid catalysts for the liquid-phase dehydration of D-xylose into furfural, J. Catal. 244 (2006) 230–237. http://www.sciencedirect.com/science/article/pii/S0021951706003228 (accessed January 27, 2014).

[29] K. Nakagawa, T. Jia, W. Zheng, S.M. Fairclough, M. Katoh, S. Sugiyama, S.C. Edman Tsang, Enhanced photocatalytic hydrogen evolution from water by niobate single molecular sheets and ensembles, Chem. Commun. 50 (2014) 13702–13705. doi:10.1039/C4CC04726E.

[30] H.T. Kreissl, K. Nakagawa, Y.-K. Peng, Y. Koito, J. Zheng, S.C.E. Tsang, Niobium oxides: Correlation of acidity with structure and catalytic performance in sucrose conversion to 5-hydroxymethylfurfural, J. Catal. 338 (2016) 329–339. doi:10.1016/j.jcat.2016.03.007.

[31] H.T. Kreissl, M.M.J. Li, Y.-K. Peng, K. Nakagawa, T.J.N. Hooper, J. V. Hanna, A. Shepherd, T.-S. Wu, Y.-L. Soo, S.C.E. Tsang, Structural Studies of Bulk to Nanosize Niobium Oxides with Correlation to Their Acidity, J. Am. Chem. Soc. 139 (2017) 12670–12680. doi:10.1021/jacs.7b06856.

[32] C.-N. Yeh, K. Raidongia, J. Shao, Q.-H. Yang, J. Huang, On the origin of the stability of graphene oxide membranes in water, Nat. Chem. 7 (2015) 166–170. doi:10.1038/nchem.2145.

[33] C.M. Tam, A.Y. Tremblay, Membrane pore characterization—comparison between single and multicomponent solute probe techniques, J. Memb. Sci. 57 (1991) 271–287. doi:10.1016/S0376-7388(00)80683-3.

[34] T. Tsuru, D. Hironaka, T. Yoshioka, M. Asaeda, Titania membranes for liquid phase separation: effect of surface charge on flux, Sep. Purif. Technol. 25 (2001) 307–314. doi:10.1016/S1383-5866(01)00057-0.

[35] N. Hilal, H. Al-Zoubi, N.A. Darwish, A.W. Mohamma, M. Abu Arabi, A comprehensive review of nanofiltration membranes:Treatment, pretreatment, modelling, and atomic force microscopy, Desalination. 170 (2004) 281–308. doi:10.1016/j.desal.2004.01.007.

Figure captions

Fig.1 TEM images and sheet size distributions of the niobate nanosheets prepared by (a) hydrothermal method and (b) exfoliation method. The sheet sizes were estimated by taking the square root of the area of each flake measured with Image J software.

Fig. 2 SEM images of overview (a, b) and cross-sections (c, d) for HT-NbO and EX-NbO membranes.

Fig. 3 XRD patterns of (a) HT-NbO and (b) EX-NbO membranes in dry and wet conditions.

Fig. 4 Water permeance and MWCO using PEG for HT-NbO and EX-NbO membranes with a thickness of 40–50 nm.

Fig. 5 Rejection of anionic dyes and salts for HT-NbO and EX-NbO membranes.

Fig. 6 (a) ζ-potentials and (b) rejection of salts as function of pH for HT-NbO and EX-NbO membranes.

Fig. 7 Schematic diagram of nanochannels in HT-NbO and EX-NbO membranes, as seen from cross-sections.

Fig. 8 Comparison of water flux behavior of (a) HT-NbO and (b) EX-NbO membranes under different pressures.

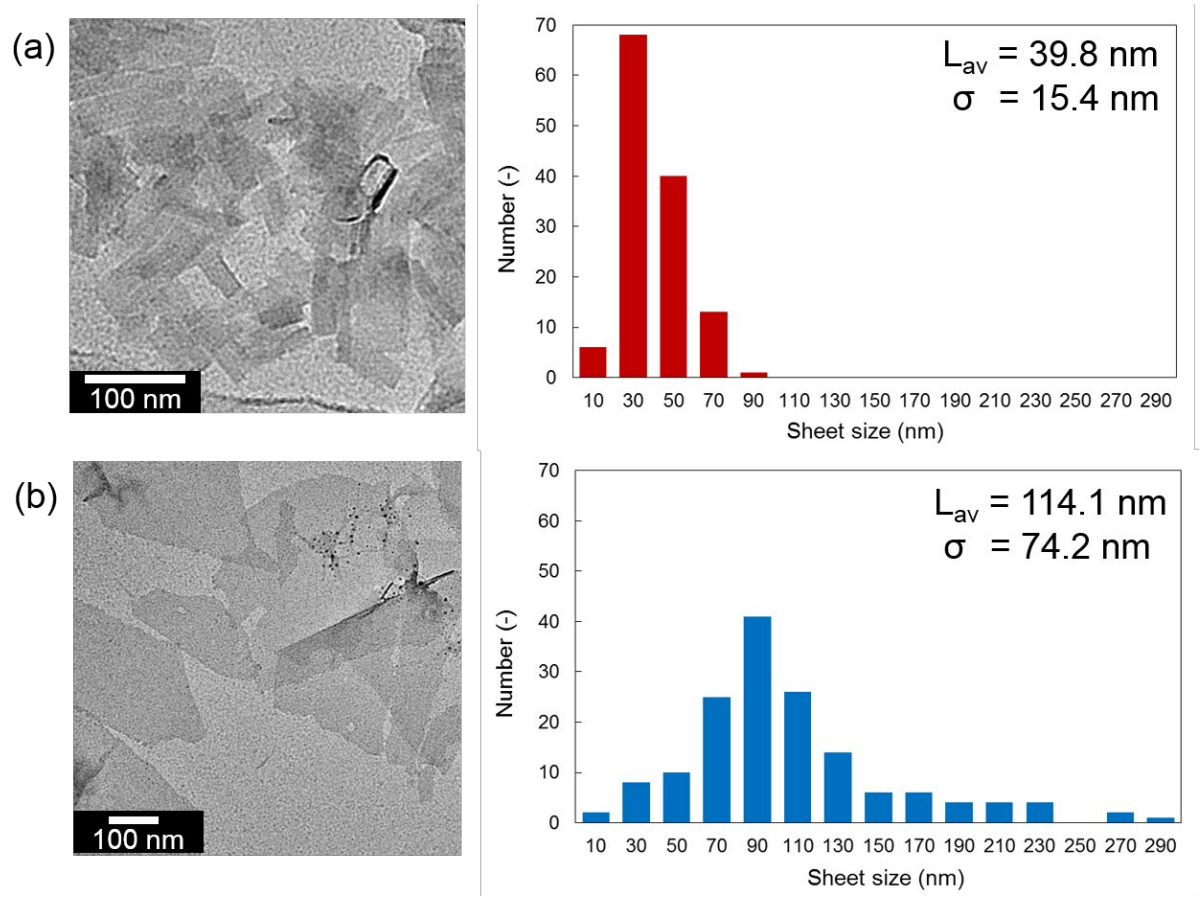

Fig.1 TEM images and sheet size distributions of the niobate nanosheets prepared by (a) hydrothermal method and (b) exfoliation method. The sheet sizes were estimated by taking the square root of the area of each flake measured with Image J software.

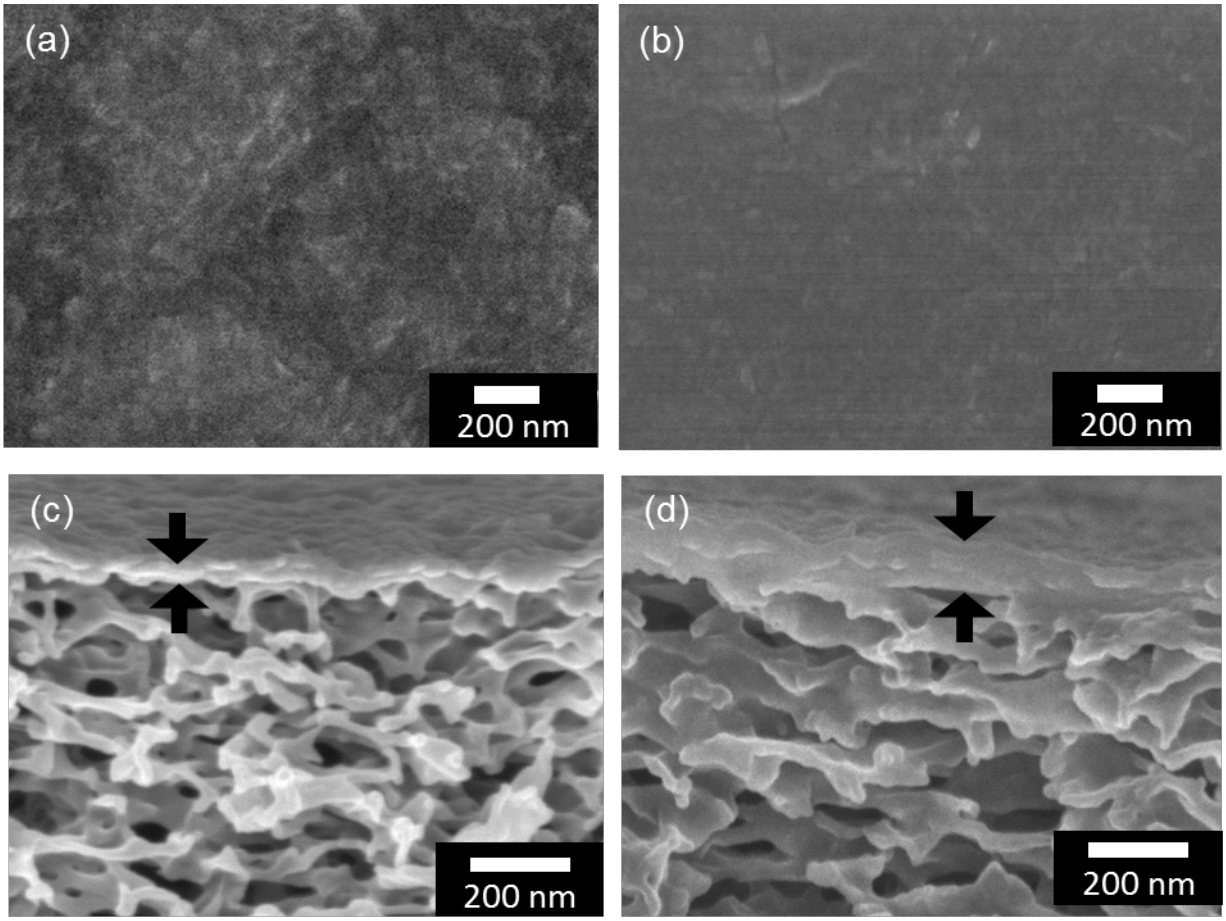

Fig. 2 SEM images of overview (a, b) and cross-sections (c, d) for HT-NbO and EX-NbO membranes.

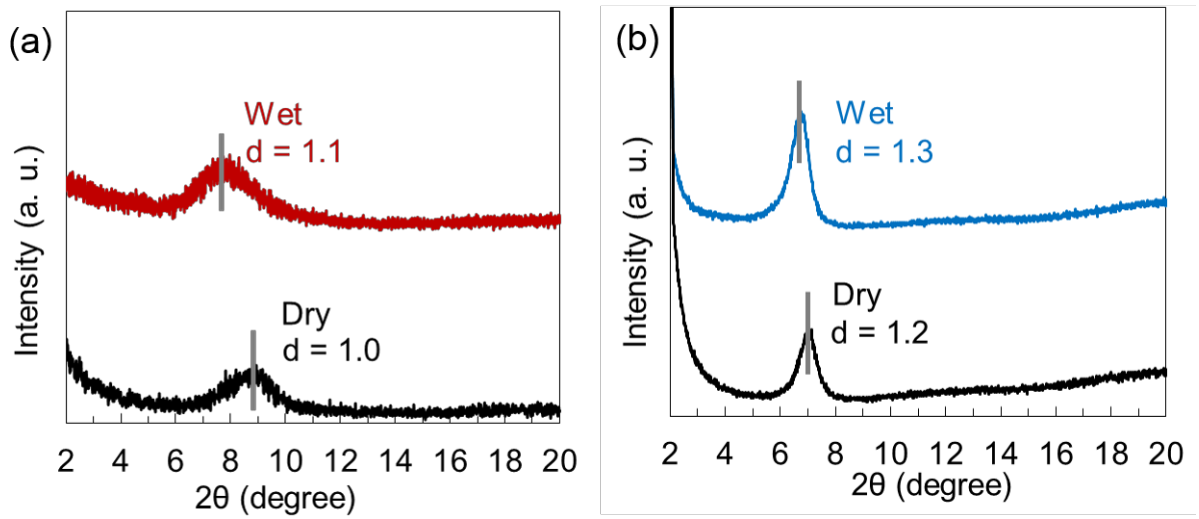

Fig. 3 XRD patterns of (a) HT-NbO and (b) EX-NbO membranes in dry and wet condition.

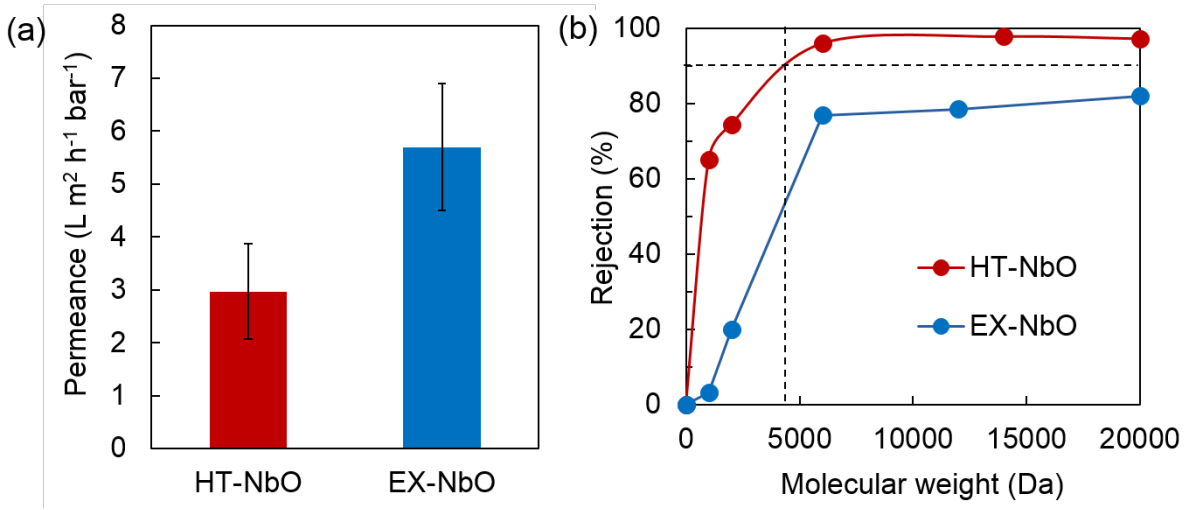

Fig. 4 Water permeance and MWCO using PEG for HT-NbO and EX-NbO membranes with a thickness of 40-50 nm.

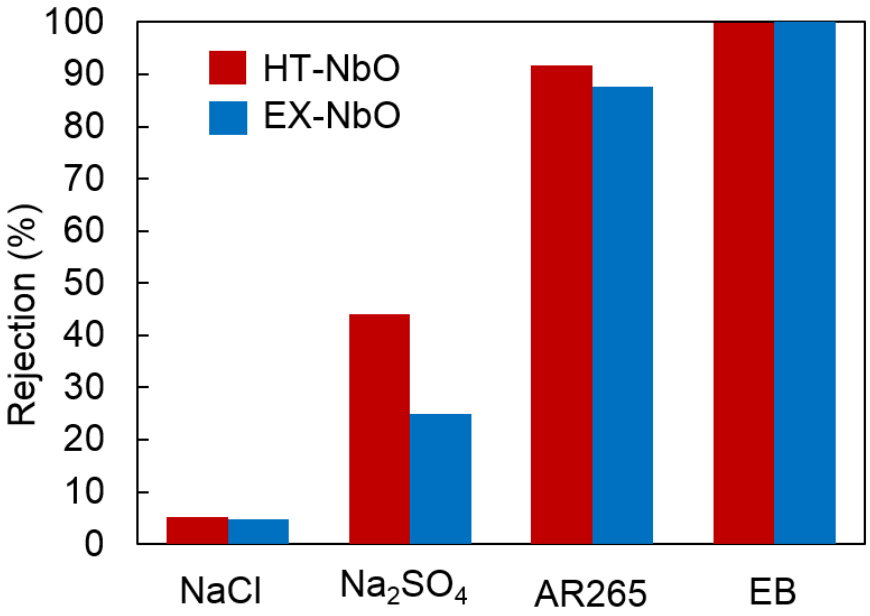

Fig. 5 Rejection of anionic dyes and salts for HT-NbO and EX-NbO membranes.

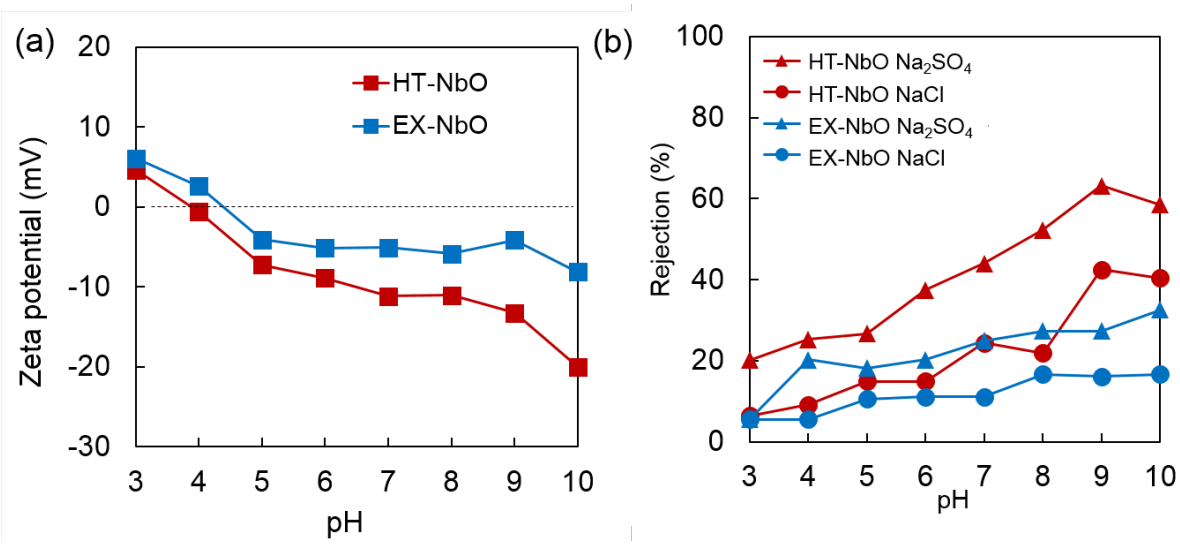

Fig. 6 (a) ζ-potentials and (b) rejection of salts as function of pH for HT-NbO and EX-NbO membranes.

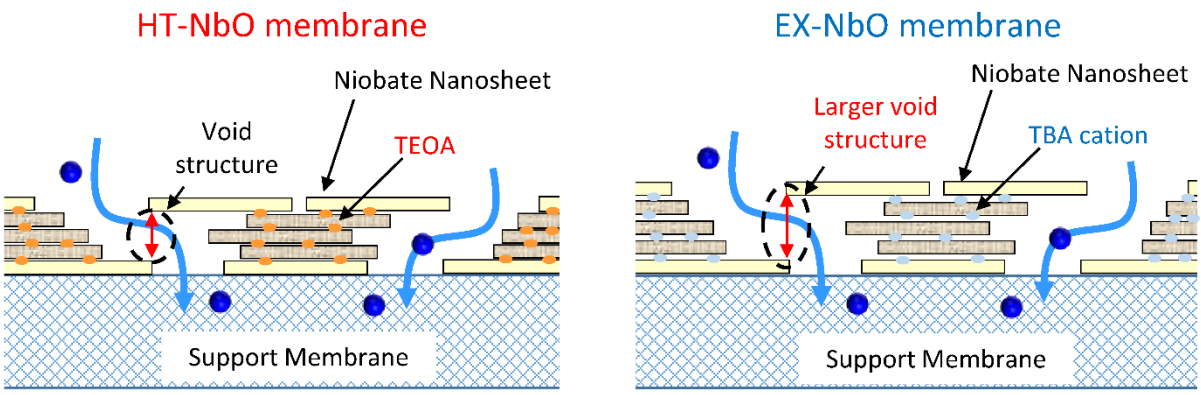

Fig. 7 Schematic diagram of nanochannels in HT-NbO and EX-NbO membranes, as seen from cross-sections.

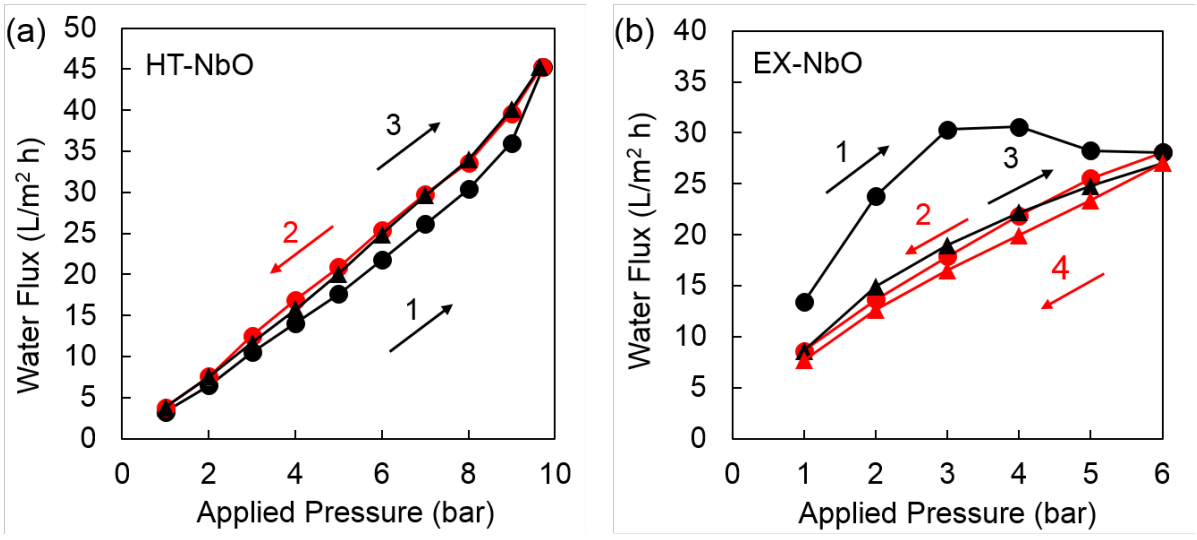

Fig. 8 Comparison of water flux behavior of (a) HT-NbO and (b) EX-NbO membranes under different pressures.